Processing and Application of Ceramics 18 [1] (2024) 87–97
https://doi.org/10.2298/PAC2401087M

Starch consolidation casting of porous alumina and functional gradient porosity development

Luiza M.C. Meira, Iricson G.A. Celestina, Christiane L. Ojaimi, Kethlinn Ramos, Adilson L. Chinelatto, Adriana S.A. Chinelatto*

PPGECM – Postgraduate Program in Materials Engineering and Science, Department of Materials Engineering, UEPG – State University of Ponta Grossa, Carlos Cavalcanti Avenue, 4748, 84030-900, Ponta Grossa PR, Brazil

Received 6 September 2023; Received in revised form 21 February 2024; Received in revised form 11 March 2024; Accepted 16 March 2024

Abstract

Starch consolidation casting (SCC) technique was successfully employed to produce both porous alumina and graded porous alumina ceramics. The solid content in the alumina suspension was maintained at 40 vol.%, with potato starch varying from 5 to 15%. Structures of the porous alumina (monolithic) samples obtained by SCC and uniaxial pressing were compared. In addition, the influence of the SCC consolidation temperature and the starch content were evaluated in the monolithic samples, while the consolidation temperature and the number of layers numbers were evaluated in the graded samples. The lower SCC consolidation temperature resulted in lower linear shrinkage and a slight increase in total porosity due to the increased pore size. The compressive strength values for the monolithic samples ranged from 60 to 200 MPa, which can be considered high when compared to previous works. The graded samples exhibited porosity variations across layers and interfaces were free of cracks and imperfections. Linear shrinkage was the same for the adopted consolidation temperature and the porosity was slightly higher for the 3-layer samples. They achieved strength of 60 MPa with fracture mode parallel to the applied load.

Keywords: *alumina, potato starch, pore network, microstructure, mechanical properties*

I. Introduction

Porous ceramic materials have numerous technological applications by leveraging the synergy between the properties of ceramics and the development of the pore network. These applications include filters [1], thermal insulators [2], catalytic supports [3], electrodes in fuel cells [4] and biomaterials [5]. Various methods are employed to achieve a specific porous structure, including sacrificial template methods [6–8], where substances used to generate pores are removed during sintering. These approaches encompass direct foaming [9], freeze casting [10], replica techniques [11], starch consolidation casting [12] and their combinations.

The starch consolidation casting (SCC) technique was introduced by Lyckfeldt and Ferreira [13] in 1998, offering significant advantages such as ease of use, compatibility with various mould materials and cost-effectiveness in terms of processing and materials. SCC involves swelling and gelatinization of starch granules, which are polysaccharides capable of forming a gel upon heating and contain components such as amylopectin and amylose [14]. The swelling of the granules occurs due to the starch's ability to absorb water from aqueous ceramic suspensions when exposed to moderate temperature, typically ranging from 55 to 80 °C [14–18]. The gelatinization process of starch granules leads to an increase in suspension viscosity and a transition to viscoelastic behaviour. The formation of a gel exerts pressure on ceramic particles, providing green strength through the formation of bonds with ceramics, acting as a binder for the particles and facilitating their consolidation into a solid body [19,20]. Therefore, starch granules serve as both pore-forming agents and body-forming components. Moreover, starch offers benefits including

* Corresponding authors: tel: +55 42 99106 7017,
e-mail: *adriana@uepg.br*

easy burnout, low cost and environmental friendliness [20,21].

Research focused on porosity achieved through starch consolidation casting has been developed, exploring its various processing parameters. Gregorová *et al.* [22] indicated that the total porosity does not correspond to the nominal starch content due to the swelling of starch in SCC. Khattab *et al.* [16] prepared porous alumina ceramics through SCC using different amounts of alumina and corn starch. Both verified that this process allowed significantly higher open porosity even at low starch contents. Nie and Lin [23] combined SCC and gel-casting techniques to produce porous alumina ceramics, achieving higher total porosity compared to those created using the traditional slip-casting method. Alumina is a common material in porous ceramics due to its excellent properties, including chemical inertness, resistance to acid corrosion and biocompatibility.

The advancement of graded pore structures, in line with the concept of functionally graded materials (FGM) [24], enables their fabrication using the SCC technique [25,26]. In this work, we investigated the influence of different processing methods (SCC and uniaxial pressing), SCC consolidation temperature and starch content on structure and properties of porous alumina ceramics. The samples were characterized in terms of linear shrinkage, porosity, microstructure and mechanical strength.

II. Experimental

2.1. Starting materials

Alumina powders CT 3000 SG from Almatis (99.8% Al_2O_3) with an average particle size of 0.5 μm and potato starch from Dinâmica Química Contemporânea (purity grade PA) with density of 1.5 g/cm^3 and water solubility of 50 g/l at 90 °C were used to prepare the suspensions. The particle size distribution was characterized using CILAS 920 particle size analyser and particle morphology was analysed using scanning electron microscopy (SEM, Tescan, Vega3). Additionally, thermogravimetric and differential thermal analysis (TG/DTA) of the potato starch was performed in air atmosphere up to 1200 °C, with a heating rate of 10 °C/min, using NETZSCH equipment, model STA 409.

Starch gelatinization process was characterized using an Olympus BX-51 optical microscope (OM). The influence of gelatinization time was evaluated in an aqueous suspension containing 40 vol.% of potato starch heated to 80 °C. Images of this suspension between glass plates were obtained at time intervals of 30, 60, 90 and 120 min.

2.2. Preparation of suspension

Suspensions were prepared for both the SCC technique and uniaxial pressing, the latter using starch as a sacrificial phase. The volume ratio of alumina and potato starch was varied (Table 1), while maintaining an overall solid volume fraction of 40%. The starch content ranged from 5 to 15 vol.%. For SCC, 0.6 vol.% of ammonium polyacrylate dispersant (Darvan 821-A) and 59.4 vol.% of water were utilized. This specific percentage of dispersant (0.6 vol.%) was identified by Almeida *et al.* [27] as suitable for the suspension, showing no significant variations in viscosity. The preparation involved ball milling for 2 h, followed by dispersion using a Sonics Vibrashock VC505 ultrasound in an ice bath for 2 min. This process comprised of cycles of 30 s with an interval of 10 s between them. For the samples obtained by uniaxial pressing, 2 wt.% of Darvan 821-A and 5 wt.% of binder (DURAMAX B1022) were included, along with ammonium hydroxide PA to stabilize the suspension.

Table 1. Sample notation and their respective compositions

Sample	Al_2O_3 [vol.%]	Potato starch [vol.%]
Al35St5	35	5
Al30St10	30	10
Al25St15	25	15

2.3. Consolidation

The SCC monolithic samples were prepared using an impermeable silicone rubber mould made to accommodate 6 cylindrical samples, each measuring 30 mm in length and 10 mm in diameter. The mould was filled with the suspension and placed in an oven at 70 and 80 °C, with each temperature maintained for 120 min. To prevent water release, the mould was covered with a plastic polyethylene film, ensuring that all the water was utilized for starch gelatinization. Subsequently, the mould was cooled to room temperature, and the samples were then extracted.

Graded samples consisting of two and three layers were also produced by SCC technique. The 2-layer samples were composed of Al35St5 and Al25St15, while the 3-layer samples included Al35St5, Al30St10 and Al25St15 layers. The assembly process involved adding equal amounts and heights of each layer in the mould. The mould was filled with the first suspension and placed in the oven at 65 °C for 10 min, after which the next layer was added. After the completing the filling, the graded samples were also placed in an oven at 70 and 80 °C, with each temperature maintained for 120 min.

For uniaxial pressing, the powders were obtained through a suspension freeze-drying process using the Lyophilizer Terroni LD1500, and then they were compacted in a cylindrical mould with diameter of 10 mm under pressure of 125 MPa.

2.4. Sintering and characterization

The sintering process was carried out in air, following a heating curve determined by TG/DTA starch analysis. Initially, the samples were heated to 180 °C at a rate of 10 °C/min and maintained at this temperature for 20 min. To remove organic compounds, the temperature

was then raised to 600 °C at a rate of 1 °C/min and held for 20 min. Subsequently, further heating was carried out to 1500 °C at a rate of 10 °C/min and maintained at this temperature for 2 h. The cooling process was conducted at a rate of 10 °C/min.

The sintered samples were characterized by linear shrinkage, with measurements taken before and after the sintering process. Porosity was assessed using three distinct methods: measurements based on the Archimedes principle following ASTM C373-18 [28], mercury porosimetry using mercury porosimeter (Autopore IV porosimeter from Micromeritics) and image analysis [29] utilizing the Image J software. The theoretical density of alumina, 3.99 g/cm^3, was employed in calculations along values obtained from bulk density and open porosity, resulting in determinations of open porosity (OP), closed porosity (CP) and total porosity (TP).

Microstructural characterization was performed on the fractured surfaces of the samples using SEM (Tescan, model Vega3). Mechanical strength was evaluated through compression tests, according to ASTM C1424-15 [30], using a universal mechanical testing machine, SHIMADZU AGI 10 KN, with a loading rate of 1 mm/min.

The results were evaluated using the analysis of variance (ANOVA) and multiple comparison tests of means, among which the Tukey test was employed. A significance level of 5% was adopted, utilizing the statistical package Action Stat, version 3.0.0 [31].

III. Results and discussion

3.1. Starting materials

Figure 1 shows the particle size distribution of alumina and potato starch particles. For alumina powders, as presented in Fig. 1a, a bimodal particle size distribution was observed, with 90% of the particles having a diameter below 4 μm, accompanied by a minor presence of particles with larger diameters. The identified average size was 3 μm, which signifies a deviation from the product's specifications. SEM image analyses displayed in Fig. 2a confirmed particles with approximately diameter size of 0.5 μm. This discrepancy observed in the particle size distribution could be attributed to the presence of agglomerates, as also demonstrated in the SEM image.

The size distribution of potato starch particles (Fig. 1b) shows that 90% of the particles have a diameter smaller than 92 μm, with an average diameter of

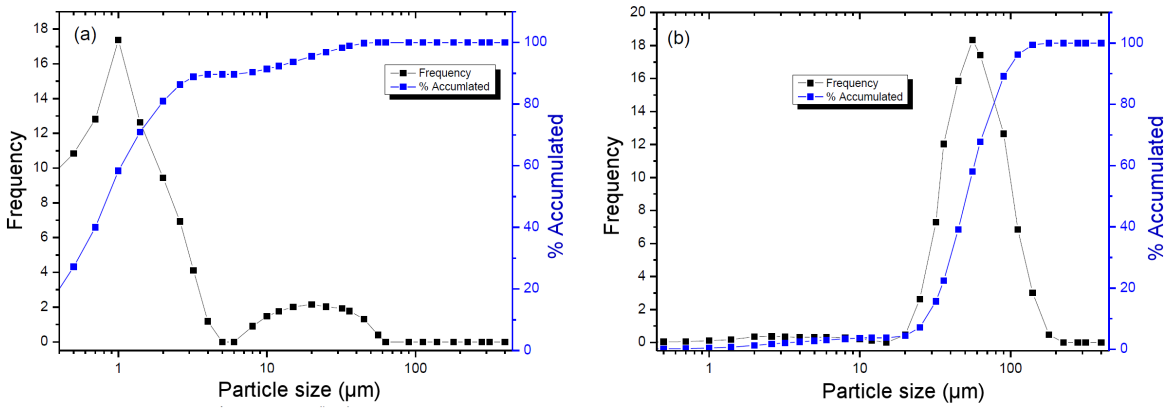

Figure 1. Particle size distribution of: a) alumina powders and b) potato starch

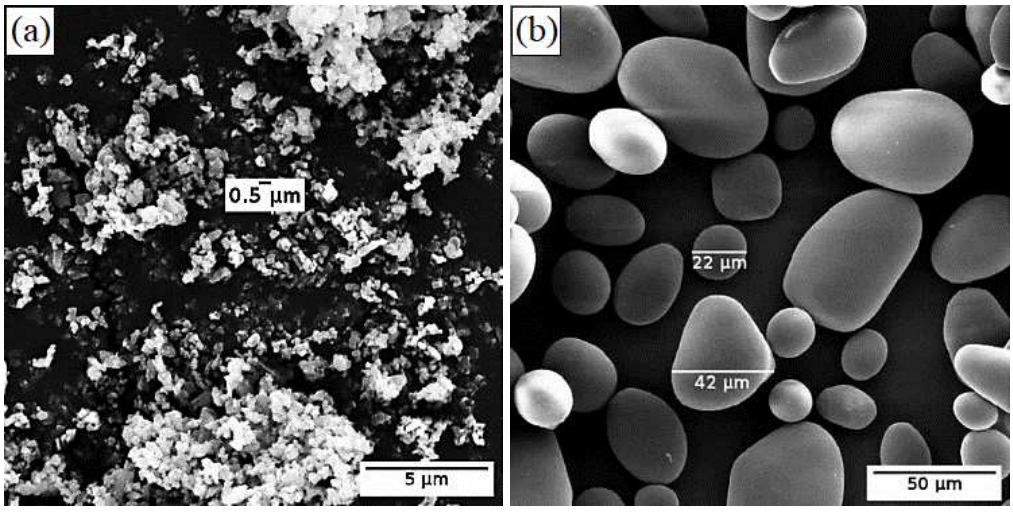

Figure 2. SEM images of: a) alumina powders and b) potato starch

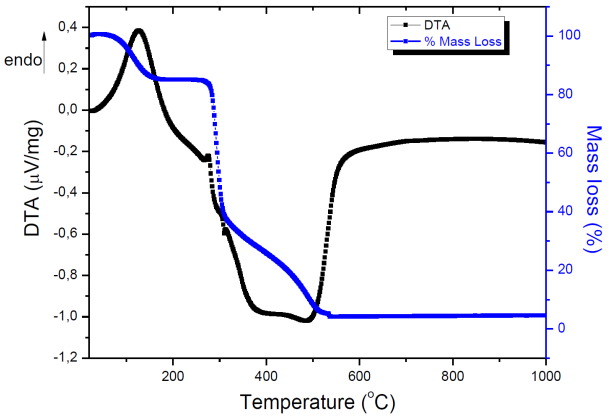

Figure 3. TG/DTA curves of potato starch

52 μm. This distribution curve exhibits a monomodal pattern. The SEM image in Fig. 2b confirms the particle size, also revealing oval or spherical morphologies. Gregorová *et al.* [32] described the different starch types concerning ceramic technologies, and both the size and shape of these particles confirm that it is indeed potato starch.

The TG and DTA profiles of potato starch are presented in Fig. 3. The TG curve displays a mass loss at a temperature close to 90 °C, accompanied by an endothermic peak in the DTA curve. These effects, observed around 100 °C, result from desorption of water. Thermal decomposition takes place between 280 and 550 °C, leading to a substantial mass loss of approximately 45%. At 280 °C, an endothermic peak appears in the DTA curve, associated with the initial decomposition process involving the combustion of starch, i.e. the cracking of amylose and amylopectin. The subsequent peaks at 380 and 500 °C represent exothermic peaks associated with the flaming combustion of gaseous products and the burning of carbonaceous residues, respectively [18,25]. According to Hórvath [33], the depolymerization of starch produces levoglucosan as a major product during starch pyrolysis. In an air atmosphere, the carbonaceous residue can react with oxygen, generating additional gases such as CO, CO_2 and water vapour. Temperatures higher than 550 °C resulted in the complete elimination of starch. Considering these observed thermal phenomena in the TG and DTA curves, heating rate of the samples within the 300 to 550 °C range must be carefully controlled during sintering to effectively manage the expulsion of breakdown products originating from potato starch.

At the beginning of the gelatinization process, the suspension containing 40 vol.% potato starch initially appeared as a white paste. When observed under an optical microscope at room temperature, as shown in Fig. 4a, the potato starch granules maintained their insolubility in water and preserved their natural state. As the temperature reached 80 °C, the suspension gradually became more swollen and voluminous; the gelatinization that transformed the paste into a gel was accompanied by the change to a transparent colour [15]. Over time, the granules increased in size and their shapes changed, as observed in Figs. 4b,c.

By analysing the optical microscope images, a significant increase in the sizes of the granules is observed when dwelling at 80 °C for 60 min, as shown in Fig. 4b. The granules swelled several times and formed a three-dimensional network [14]. As time progressed to 120 min, as depicted in Fig. 4c, the interaction between these swollen particles intensified, resulting in the breakdown of gelled molecules due to the increased interaction. Consequently, the swollen granules began to rupture and collapse [19].

The potato starch was compared with other types of starches [14,19,20,34]. Živcová *et al.* [18] utilized a swelling kinetic model to estimate the required time for consolidation, considering the maximum packing fraction achievable by compressing the ceramic powder. Under these conditions, potato starch demonstrated faster swelling and more effective consolidation compared to other starch types. Despite potato starch exhibiting rapid swelling, time periods longer than 1 h are necessary due to the rheological changes in the suspension. These changes promote the strength and rigidity for better properties of ceramic green bodies [18,20].

3.2. Porous alumina samples

The linear shrinkage measurements of the sintered monolithic samples, consolidated at temperatures of 70 and 80 °C for 120 min, as well as the samples obtained by uniaxial pressing using starch as a sacrificial phase, are shown in Fig. 5. Since the sintering curve was the same for all samples, the differences observed in linear shrinkage were a reflection of the consolidation method

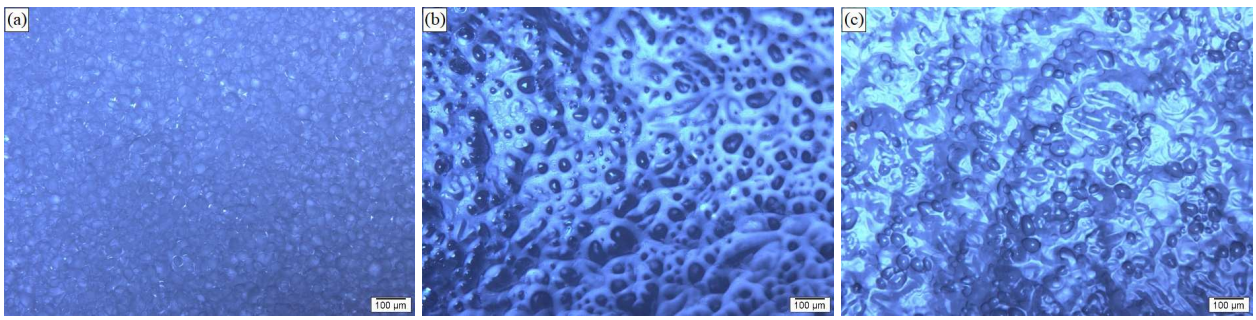

Figure 4. Optical microscope images of starch gelatinization obtained in transmittance mode at: a) room temperature, b) 60 min at 80 °C and c) 120 min at 80 °C

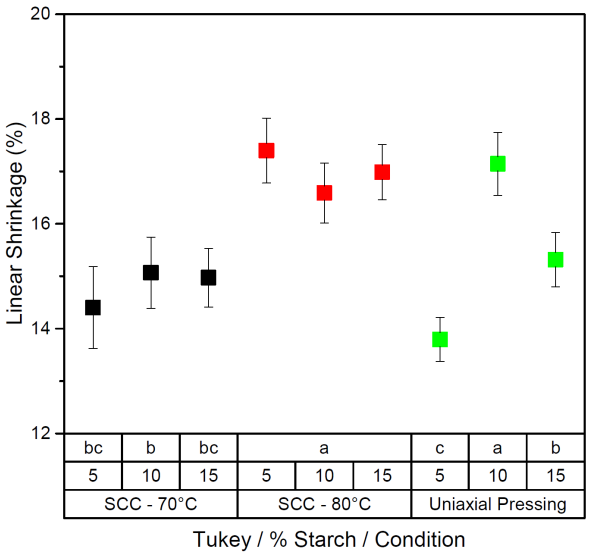

Figure 5. Linear shrinkage of sintered monolithic samples prepared by SCC at 70 and 80 °C and by uniaxial pressing (Tukey test - compositions and sintering conditions followed by the same letter do not differ)

and/or the amount of starch. For the samples consolidated by SCC at 70 °C, linear shrinkage values ranged from 14.4% to 15.0%, while at 80 °C, they ranged from 16.5% to 17.4%. The Tukey test revealed the presence of statistical differences in the consolidation temperature, indicating that the shrinkage was dependent on the consolidation temperature used, which, in turn, directly affects the pore size. Furthermore, there was relative independence regarding the amount of potato starch for the samples consolidated by SCC. For the uniaxially pressed samples, shrinkage should have been lower due to the formation of pores resulting solely from burning of potato starch as a sacrificial phase, which did not happen. Moreover, there was also no dependence on the amount of starch.

The linear shrinkage did not correlate with the amount of starch, in agreement with literature [19,22,23,35,36]. In SCC process, large pores are formed due to the starch swelling, and these do not contribute to the shrinkage during the sintering mechanism; instead, only the ceramic matrix is responsible for this. The difference in linear shrinkage according to SCC temperature can be attributed to the difference in packing of the alumina particles, as well as the solid content [22]. The processing temperature influenced the swelling of the starch, impacting particle packing.

Figure 6 compares the average values of open, closed and total porosities obtained for the sintered monolithic samples, along with the Tukey test results. The open porosity increased with higher amounts of potato starch. Notably, closed porosity appeared smaller than open porosity, indicating three-dimensionally connected pores (large pores connected by passages of small pores). Consequently, the total porosity was higher for the samples consolidated by SCC due to the swelling and gelatinization process of starch, resulting in larger pore sizes [17]. When comparing samples produced via SCC, the TP resulted in higher values for consolidation at 70 °C, confirmed by the Tukey test, suggesting that gelatinization might have occurred without the breakdown of starch molecules, resulting in larger pores [22]. For the samples produced by uniaxial pressing, the porosities were higher than expected. This increased porosity may be attributed to the incomplete densification of alumina [13], presenting higher values of porosity than the nominal concentration of starch. SEM image (Fig. 7) confirmed the presence of porosity in the alumina matrix.

SEM images of the Al35St5 and Al25St15 samples are shown in Fig. 8. A significant difference in pore morphology is noticeable between the samples obtained by SCC and those uniaxially pressed using starch solely as a sacrificial template. The contrasting pore structure obtained by SCC emphasizes the processing technique, revealing the development of a shell-like structure within the pores, likely resulting from potato starch combustion [16]. In pressed samples, the pores retain a similar size, with an increase in the number of pores with an increasing amount of starch, leading to the presence of agglomerates and generating some larger pores.

As shown in Fig. 6, an increase in the amount of starch led to higher porosity. Moreover, this increase

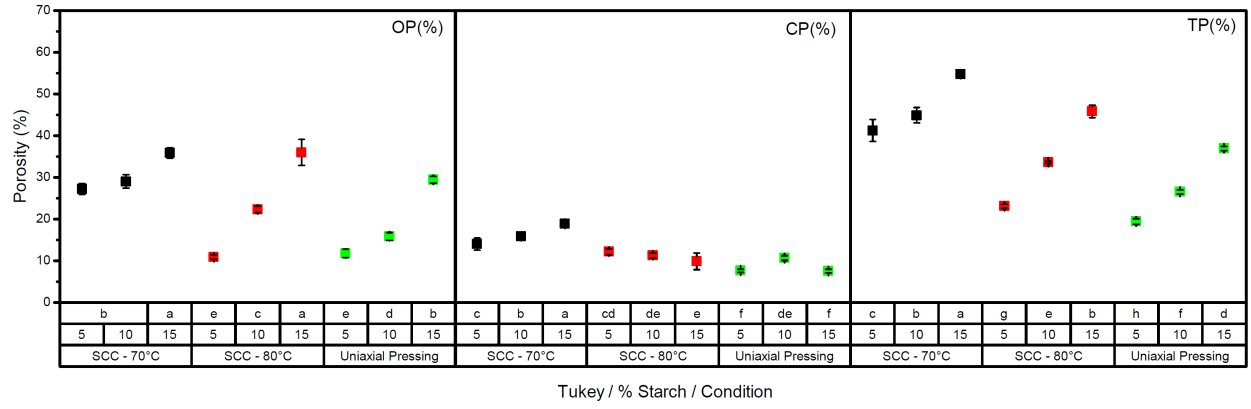

Figure 6. Open porosity (OP), closed porosity (CP) and total porosity (TP) for the sintered monolithic samples consolidated by SCC at 70 and 80 °C and uniaxial pressing (Tukey test - compositions and sintering conditions followed by the same letter do not differ)

was correlated with the pore size, as revealed in Fig. 9, which shows the average pore diameter measured through image analysis. Higher starch content is associated with an increase in pore size due to the interaction between starch particles. The number and degree of contact between the starch particles contribute to the development of open pathways and channels among pores, resulting in larger average pore size and higher porosity [27]. Another observed factor was an increase in pore

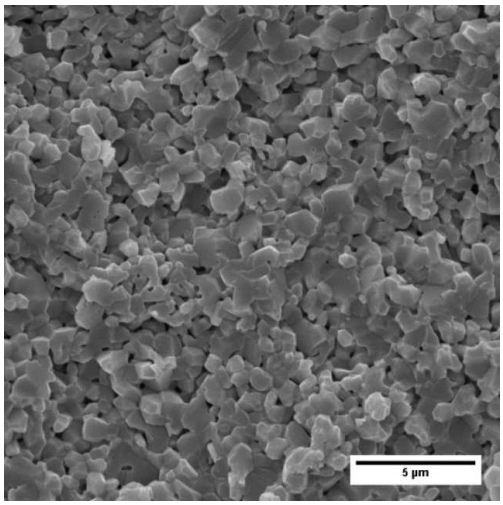

Figure 7. SEM image of alumina matrix

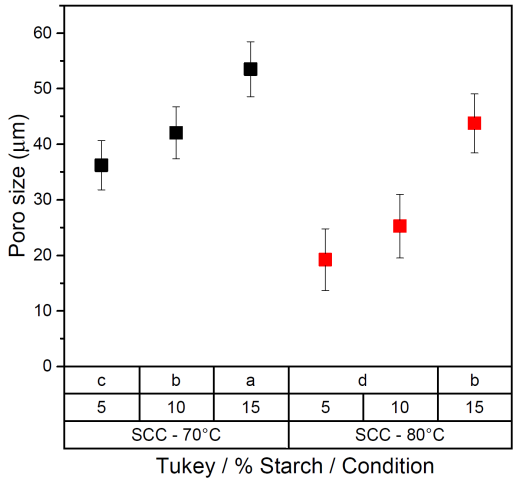

Figure 9. Average pore size of the sintered samples consolidated by SCC at temperatures of 70 and 80 °C

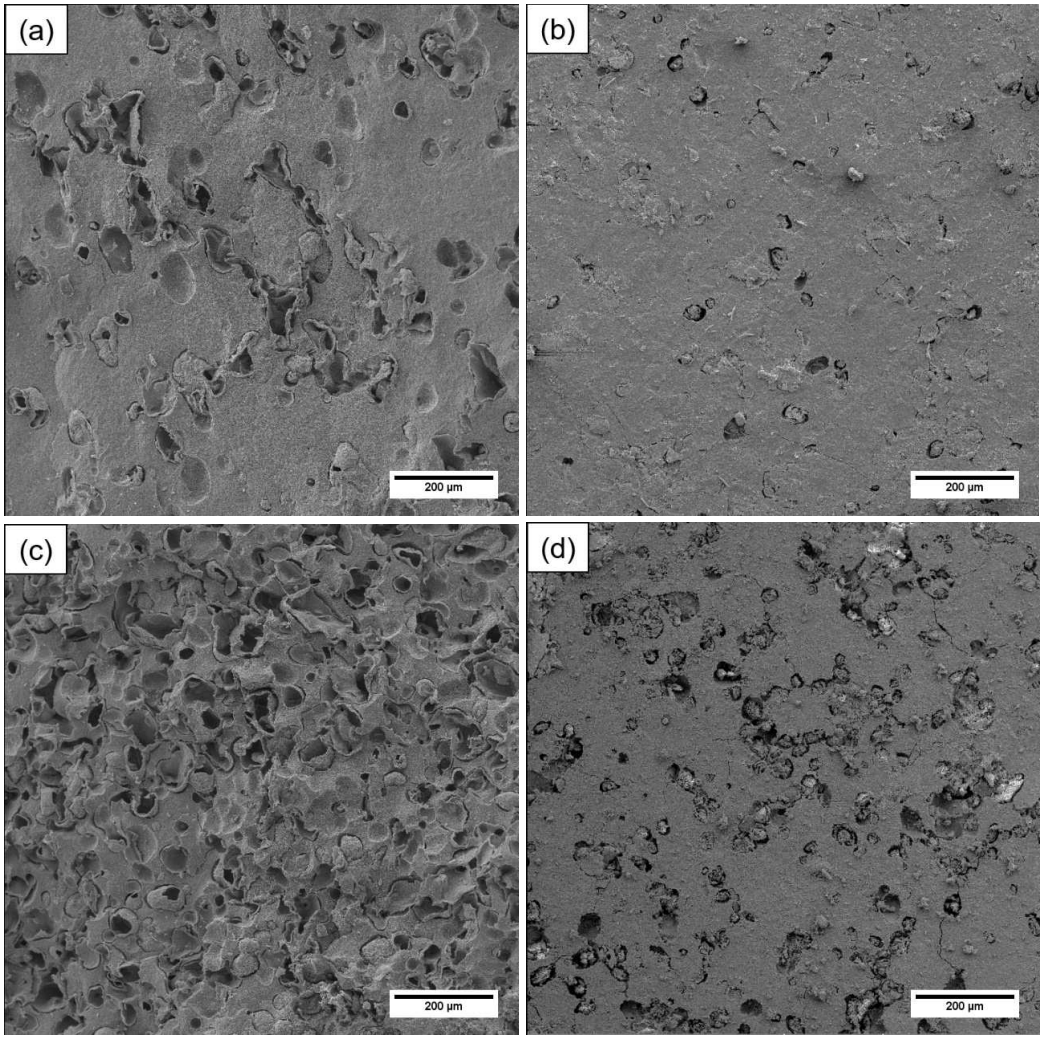

Figure 8. SEM images of the sintered Al35St5 consolidated by SCC at 70 °C (a) and by uniaxial pressing (b), and Al25St15 consolidated by SCC at 70 °C (c) and by uniaxial pressing (d)

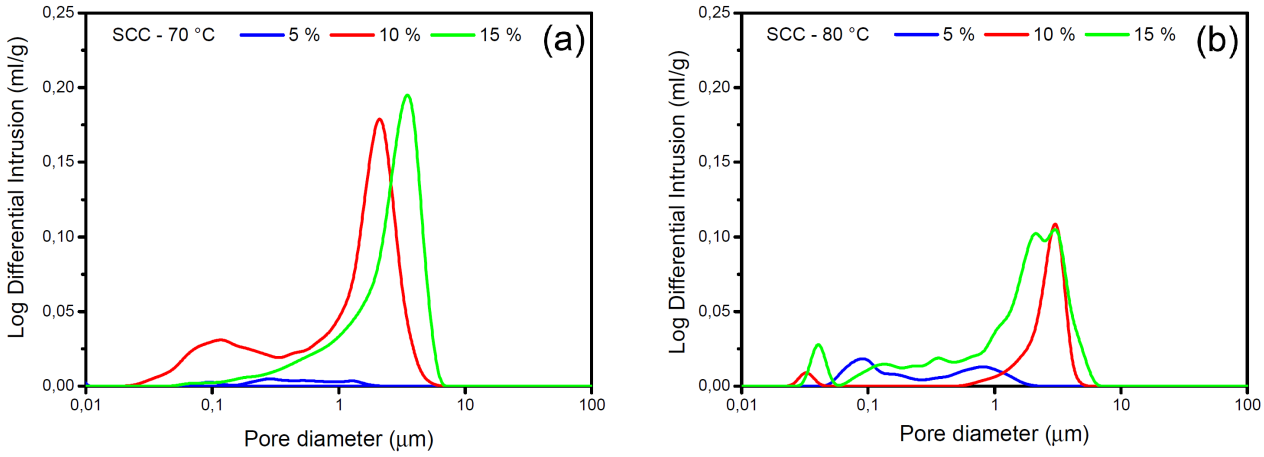

Figure 10. Pore diameter obtained through mercury porosimetry for Al35St5, Al30St10 and Al25St15 consolidated at: a) 70 and b) 80 °C

size at a lower gelatinization temperature, 70 °C, which would justify higher values of total porosity and lower linear shrinkage.

The pore diameter measurements obtained through mercury intrusion porosimetry are depicted in Fig. 10, revealing a bimodal pore size distribution. The pore size corresponding to the first peak is likely attributed to the porosity of a partially sintered matrix, representing the smallest pore population [37]. Values around 0.1 μm were observed for the samples Al30St10 consolidated at 70 °C and less than 0.1 μm for those Al30St10 and Al25St15 consolidated at 80 °C. The second peak indicates the interconnection between the cavities formed by the starch [37], with both samples with 10% and 15% of starch consolidated at 70 and 80 °C presenting values between 0.3 and 7 μm. Despite slight differences in the average sizes for the second peak, they are still relatively close, suggesting the presence of interconnections with similar dimensions [38].

It is interesting to note that the pore sizes were much smaller when measured by mercury porosimetry than those observed in SEM images. This is because mercury porosimetry indicates the size of small-diameter channels interpreted as pore throat size distributions or cell window diameters. In contrast, SEM shows that larger pores formed as a result of the swelling and burning out of starch granules during sintering [17,25,35,36,39,40].

When assessing the SCC samples for mechanical strength, the results presented in Fig. 11 indicated a reduction in strength with an increase in porosity, characterized by the quantity of added potato starch. When comparing samples with the same amount of starch consolidated at different temperatures, the increase in porosity for samples consolidated at 70 °C, as shown in Fig. 6, as well as the higher pore size, as shown in Fig. 9, resulted in a reduction in compressive strength. Under compression, the crack propagation in the ceramic body occurs slowly, and the fracture is related to the average crack size. Thus, ceramic bodies with higher density and smaller pore sizes exhibit higher compressive strength [7].

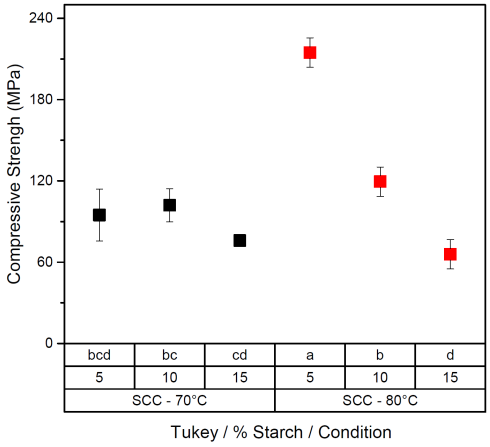

Figure 11. Compressive strength of monolithic samples consolidated by SCC at temperatures of 70 and 80 °C (compositions followed by the same letter do not differ)

The compressive strength reached values ranging from 60 MPa to 200 MPa, considering their respective porosities (Fig. 6). These values can be considered high when compared to previous works. Pagano *et al.* [14] reported ~25 MPa for the samples of similar composition produced by freeze casting. Furthermore, Nie and Lin [23] achieved 24 MPa by combining starch consolidation with the gel casting process for alumina samples with 10 vol.% starch. This suggests that processing through SCC, with the same composition and amount of starch, produces pore shapes that probably result in greater mechanical resistance.

The fracture mode occurred with the origin parallel to the load application, as shown in Fig. 12. Brittle ceramics undergo compression failure through a process of progressive microfracture, where microcracks grow and form failure planes [42]. In compression, small cracks extend stably, growing with increasing stress until they interact and cooperate to cause final failure [43,44]. As reported by Meile *et al.* [43], Al_2O_3 with porosities below 50% exhibits brittle fracture with the propagation of long cracks parallel to the loading direction, which was also demonstrated in this work.

Figure 12. Fracture mode in Al35St5 sample consolidated by SCC at 70 °C

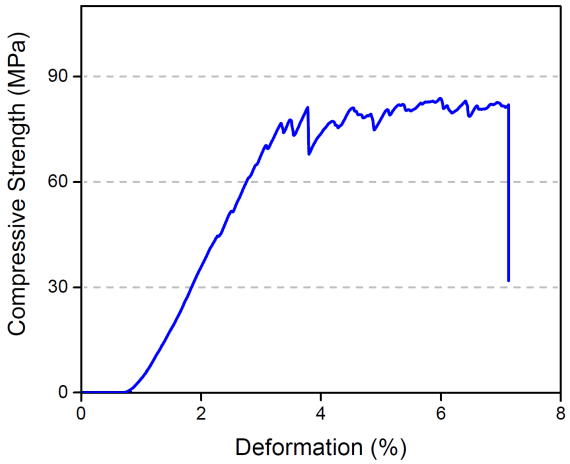

Figure 13. Typical stress-strain curves of porous samples, specifically in Al25St15 consolidated at 70 °C

However, an interesting observation is the "kneading" phenomenon, highlighted in Fig. 12, indicating the toughening of the sample at the beginning of the load application. This phenomenon was also evident in the tension versus deformation curves, as represented in Fig. 13. Initially, there is a region of linear elastic deformation, which then deviates from linearity, displaying small steps in the curve and forming a plateau with successive steps. The observed load drops may be associated with the propagation of small cracks in the ceramics, attributed to the progressive collapse of the solid phase between the pores [43]. In porous materials, microcracking is associated with the failure of the microstructural elements, facilitated by the presence of a large number of pores [35]. This behaviour was similar for all the samples.

3.3. Graded samples

Figure 14 shows the graded samples with 2 layers (Al35St5 and Al25St15) and 3 layers (Al35St5, Al30St10 and Al25St15) consolidated at 80 °C, emphasizing the interface between layers and the integrity of the samples. In Fig. 14b, at higher magnification, differences in porosity were noted. Additionally, there was no evidence of cracks or macroscopic divisions between

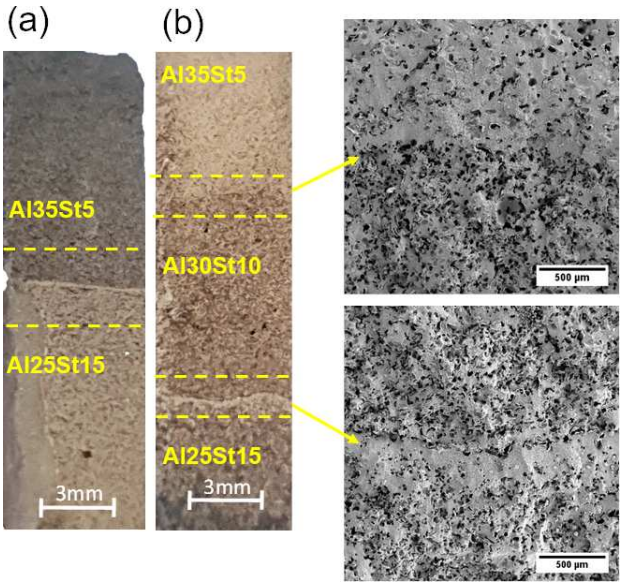

Figure 14. SEM images of graded samples with: a) 2 layers and b) 3 layers

the layers or abrupt interface separating them, which increases the reliability of the system. Gregorová *et al.* [25] also successfully produced a functional gradient material with a pore-size gradient, even though they employed different types of starch.

The linear shrinkage measurements for the sintered graded samples were very similar. For the 2-layer samples consolidated at 70 °C, the linear shrinkage was 15% and at 80 °C it was 14%, whereas, for the 3-layer samples consolidated at 70 °C, the linear shrinkage was 15% and at 80 °C it was 14%. As the linear shrinkage showed no statistical difference with the amount of starch in the monolithic samples (Fig. 5), in the graded samples this behaviour was beneficial in preventing failures between the layers. Considering the consolidation temperatures in the graded samples, there was no difference in shrinkage between them.

Figure 15 presents the values of OP, CP and TP of the 2- and 3-layer graded samples consolidated by SCC at 70 and 80 °C. No statistical difference in open porosity was observed among the samples, regardless of the consolidation temperature or number of layers. However, close and total porosities for the samples consolidated at 80 °C resulted in higher values compared to those consolidated at 70 °C. Furthermore, the porosities in the layered samples exhibited higher overall values compared to the monolithic samples (Fig. 6). Gregorová *et al.* [26] reported that a partial confinement, typical for the processing of layered laminates, which involves a large free surface, allows swelling in the normal direction to the free surface.

The compressive strength results for the 2- and 3-layer samples consolidated at 70 and 80 °C are presented in Fig. 16. No significant variation was observed in the compressive strength values among the samples. The stress-strain curves exhibited a similar behaviour with those shown in Fig. 13. This similarity between

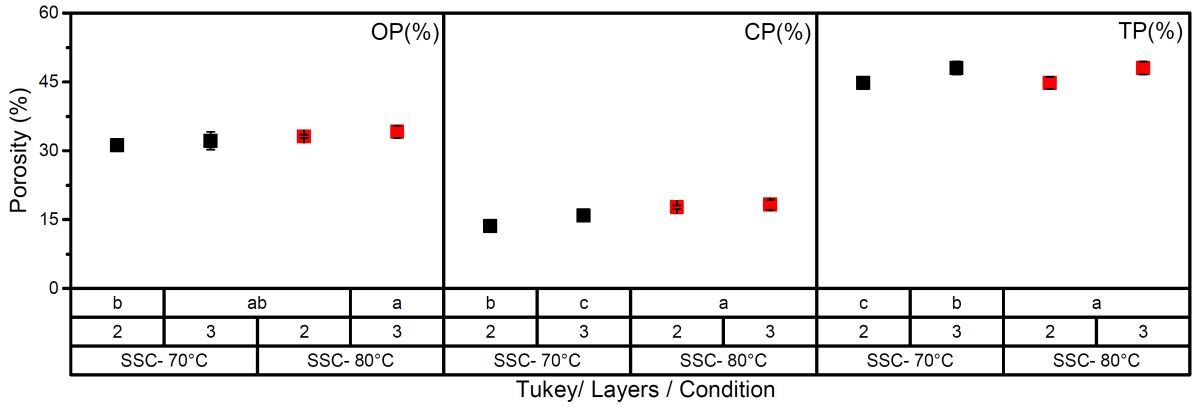

Figure 15. Open porosity (OP), close porosity (CP) and total porosity (TP) of 2- and 3-layer graded samples (averages followed by the same letter, for the same porosity, do not differ)

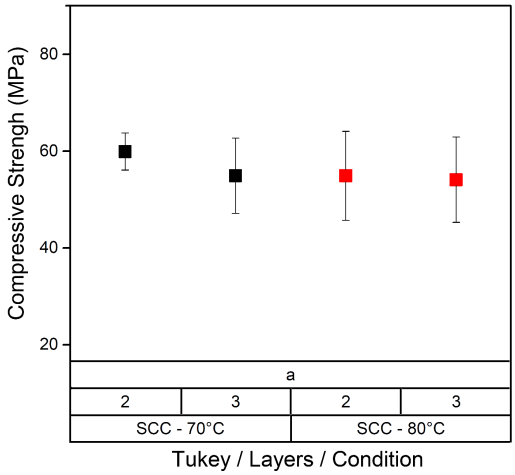

Figure 16. Compressive strength of graded samples consolidated by SCC at temperatures of 70 and 80 °C (compositions followed by the same letter do not differ)

the monolithic and graded samples suggests a fracture mechanism involving sequential microcracks for both systems [35].

Furthermore, similar to the monolithic samples, fractures in the layered samples also occurred parallel to the load application. This is noteworthy since fractures and cracks often could develop at the interface between layers. Another advantage of the graded samples was the longer time required until catastrophic failure occurs. The layers delayed fracture by significantly increasing the kneading in samples.

IV. Conclusions

Monolithic and graded porous alumina samples were produced using starch consolidation casting, yielding excellent mechanical strength. Porosity resulting from the SCC increased with the amount of potato starch, while linear shrinkage was not correlated with the starch amount but rather with the consolidation temperature adopted. In comparison, monolithic samples produced by uniaxial pressing using starch as the sacrificial phase exhibited total porosity levels higher than expected, possibly due to pores within the alumina matrix. SEM images underscored the influence of the consolidation technique and the amount of starch on the pore morphology and size. Layered samples with a porosity gradient were obtained simply and effectively. Regarding porosity, lowering the gelatinization temperature in the SCC process from 80 to 70 °C did not result in significant differences in total porosity for both 2- and 3-layer samples. This suggests that starch gelatinization and pore growth occurred with minimal pore breakage and interconnectivity changes. These graded samples demonstrated structural integrity and favourable mechanical properties (~60 MPa), highlighting the potential of this approach to achieve high strength with controlled porosity.

Acknowledgements: This work was supported by the Coordenação de Aperfeiçoamento de Pessoal de Nível Superior – Brasil (CAPES) – Finance Code 001; the Conselho Nacional de Desenvolvimento Científico e Tecnológico (CNPq); the Fundação Araucária de Apoio do Desenvolvimento Científico e Tecnológico do Estado do Paraná; and Almatis do Brasil Ltda.

References

1. B. Ren, Y. Wang, J. Liu, X. Zhang, Y. Chen, Y. Rong, J. Yang, "Preparation of Al_2O_3-Si_3N_4 porous ceramics with a cactus-like architecture for potential filters applications", *Ceram. Int.*, **45** [5] (2019) 6581–6584.
2. S. Rajpoot, R. Malik, Y.W. Kim, "Low thermal conductivity in porous SiC-SiO_2-Al_2O_3-TiO_2 ceramics induced by multiphase thermal resistance", *Ceram. Int.*, **47** [14] (2021) 20161–20168.
3. C. Quan, N. Gao, C. Wu, "Utilization of NiO/porous ceramic monolithic catalyst for upgrading biomass fuel gas", *J. Energy Inst.*, **91** [3] (2018) 331–338.
4. N. Hedayat, Y. Du, H. Ilkhani, "Review on fabrication techniques for porous electrodes of solid oxide fuel cells by sacrificial template methods", *Renew. Sustain. Energy Rev.*, **77** (2017) 1221–1239.
5. F. Baino, M. Ferraris, "Learning from nature: Using bioinspired approaches and natural materials to make porous bioceramics", *Int. J. Appl. Ceram. Technol.*, **14** [4] (2017) 507–520.

6. J. Liu, B. Ren, Y. Lu, X. Xi, Y. Li, K. Liu, J. Yang, Y. Huang, "Novel design of elongated mullite reinforced highly porous alumina ceramics using carbonized rice husk as pore-forming agent", *Ceram. Int.*, **45** [11] (2019) 13964–13970.
7. M. Zhang, X. Li, M. Zhang, Z. Xiu, J.-G. Li, J. Li, M. Xie, J. Chen, X. Sun, "High-strength macro-porous alumina ceramics with regularly arranged pores produced by gel-casting and sacrificial template methods", *J. Mater. Sci.*, **54** [14] (2019) 10119–10129.
8. A. Çelik, G. Çağlar, Y. Çelik, "Fabrication of porous Al_2O_3 ceramics using carbon black as a pore forming agent by spark plasma sintering", *Ceram. Int.*, **48** [19] (2022) 28181–28190.
9. Z. Du, D. Yao, Y. Xia, K. Zuo, J. Yin, H. Liang, Y.P. Zeng, "Highly porous silica foams prepared via direct foaming with mixed surfactants and their sound absorption characteristics", *Ceram. Int.*, **46** [9] (2020) 12942–12947.
10. F. Ye, J. Zhang, L. Liu, H. Zhan, "Effect of solid content on pore structure and mechanical properties of porous silicon nitride ceramics produced by freeze casting", *Mater. Sci. Eng. A*, **528** [3] (2011) 1421–1424.
11. A.D.R. Silva, W.R. Rigoli, D. Osiro, D.C.R. Mello, L.M.R. Vasconcellos, A.O. Lobo, E.M.J.A. Pallone, "Surface modification using the biomimetic method in alumina-zirconia porous ceramics obtained by the replica method", *J. Biomed. Mater. Res. Part B Appl. Biomater.*, **106** [7] (2018) 2615–2624.
12. Z. Chen, G. Xu, H. Cui, X. Zhang, X. Zhan, "Preparation of porous Al_2O_3 ceramics by starch consolidation casting method," *Int. J. Appl. Ceram. Technol.*, **15** [6] (2018) 1550–1558.
13. O. Lyckfeldt, J.M.F. Ferreira, "Processing of porous ceramics by 'starch consolidation'", *J. Eur. Ceram. Soc.*, **18** [2] (1998) 131–140.
14. M.H. Talou, M.A. Villar, M.A. Camerucci, R. Moreno, "Rheology of aqueous mullite-starch suspensions", *J. Eur. Ceram. Soc.*, **31** [9] (2011) 1563–1571.
15. T. Zhu, Y. Wang, "Alumina ceramics fabricated by in-situ consolidation of pre-gelling starch", *J. Wuhan Univ. Technol. Mater. Sci. Ed.*, **33** [3] (2018) 758–766.
16. R.M. Khattab, M.M.S. Wahsh, N.M. Khalil, "Preparation and characterization of porous alumina ceramics through starch consolidation casting technique", *Ceram. Int.*, **38** [6] (2012) 4723–4728.
17. E. Gregorová, W. Pabst, "Process control and optimized preparation of porous alumina ceramics by starch consolidation casting", *J. Eur. Ceram. Soc.*, **31** [12] (2011) 2073–2081.
18. Z. Živcová, E. Gregorová, W. Pabst, "Low- and high-temperature processes and mechanisms in the preparation of porous ceramics via starch consolidation casting", *Starch*, **62** [1] (2010) 3–10.
19. L.B. Garrido, M.P. Albano, L.A. Genova, K.P. Plucknett, "Influence of starch type on characteristics of porous 3Y-ZrO_2 prepared from a direct consolidation casting method", *Mater. Res.*, **14** [1] (2011) 39–45.
20. M.H. Talou, M.A. Villar, M.A. Camerucci, "Thermogelling behaviour of starches to be used in ceramic consolidation processes", *Ceram. Int.*, **36** [3] (2010) 1017–1026.
21. M.M. Lorente-Ayza, S. Mestre, V. Sanz, E. Sánchez, "On the underestimated effect of the starch ash on the characteristics of low cost ceramic membranes", *Ceram. Int.*, **42** [16] (2016) 18944–18954.
22. E. Gregorová, Z. Živcová, W. Pabst, "Porosity and pore space characteristics of starch-processed porous ceramics", *J. Mater. Sci.*, **41** [18] (2006) 6119–6122.
23. Z. Nie, Y. Lin, "Fabrication of porous alumina ceramics with corn starch in an easy and low-cost way", *Ceram. Silikaty*, **59** [4] (2015) 348–352.
24. M. Naebe, K. Shirvanimoghaddam, "Functionally graded materials: A review of fabrication and properties", *Appl. Mater. Today*, **5** (2016) 223–245.
25. E. Gregorová, Z. Živcová, W. Pabst, "Porous ceramics made using potato starch as a pore-forming agent", *Fruit Veget. Cereal Sci. Biotechnol.*, **3** [1] (2009) 115–127.
26. E. Gregorová, W. Pabst, M. Chmelíčková, "Layered alumina ceramics with porosity steps," *Adv. Sci. Technol.*, **63** (2010) 364–369.
27. F.A. Almeida, E.C. Botelho, F.C.L. Melo, T.M.B. Campos, G.P. Thim, "Influence of cassava starch content and sintering temperature on the alumina consolidation technique", *J. Eur. Ceram. Soc.*, **29** [9] (2009) 1587–1594.
28. ASTM International, "ASTM C373-18: Standard test methods for determination of water absorption and associated properties by vacuum method for pressed ceramic tiles and glass tiles and boil method for extruded ceramic tiles and non-tile fired ceramic whiteware products", *ASTM Int.*, **18** (2016) 5.
29. C.A. Schneider, W.S. Rasband, K.W. Eliceiri, "NIH Image to ImageJ: 25 years of image analysis", *Nat. Methods*, **9** [7] (2012) 671–675.
30. ASTM International, "Standard test method for monotonic compressive strength of advanced ceramics at ambient temperature", *ASTM Int.*, **08** (2010) 1.
31. *Action Stat Software*, version 3.0.0, EstatCamp, Brasil, https://www.estatcamp.com.
32. E. Gregorová, W. Pabst, I. Bohačenko, "Characterization of different starch types for their application in ceramic processing", *J. Eur. Ceram. Soc.*, **26** [8] (2006) 1301–1309.
33. E. Horváth, "Thermal analysis of starch for realizing embedded channel in low temperature co-fired ceramic", *J. Therm. Anal. Calorim.*, **114** [1] (2013) 277–284.
34. M.L. Sandoval, M.H. Talou, A.G. Tomba Martinez, M.A. Camerucci, E. Gregorová, W. Pabst, "Starch consolidation casting of cordierite precursor mixtures-rheological behavior and green body properties", *J. Am. Ceram. Soc.*, **98** [10] (2015) 3014–3021.
35. M.L. Sandoval, M.H. Talou, A.G. Tomba Martinez, M.A. Camerucci, E. Gregorová, W. Pabst, "Porous cordierite-based ceramics processed by starch consolidation casting – Microstructure and high-temperature mechanical behavior", *Ceram. Int.*, **44** [4] (2018) 3893–3903.
36. Z. Živcová-Vlčkova, J. Locs, M. Keuper, I. Sedlářová, M. Chmelíčková, "Microstructural comparison of porous oxide ceramics from the system Al_2O_3-ZrO_2 prepared with starch as a pore-forming agent", *J. Eur. Ceram. Soc.*, **32** [10] (2012) 2163–2172.
37. R. Ahmad, M.S. Anwar, J. Kim, I.H. Song, S.Z. Abbas, S.A. Ali, F. Ali, J. Ahmad, H. Bin Awais, M. Mehmood, "Porosity features and gas permeability analysis of bimodal porous alumina and mullite for filtration applications", *Ceram. Int.*, **42** [16] (2016) 18711–18717.
38. S. Li, C.-A. Wang, J. Zhou, "Effect of starch addition on microstructure and properties of highly porous alumina ce-

ramics", *Ceram. Int.*, **39** [8] (2013) 8833–8839.
39. R.A. Shakir, R. Géber, "Structure and properties of ZrO_2-Al_2O_3-MgO porous ceramic for biomedical applications", *Results Eng.*, **18** (2023) 101104.
40. Z. Zivcová, E. Gregorová, W. Pabst, "Alumina ceramics prepared with new pore-forming agents", *Process. Appl. Ceram.*, **2** [1] (2008) 1–8.
41. E. Pagano, A.S.A. Chinelatto, A.L. Chinelatto, "Freeze casting process for the generation of graded porosity in Al_2O_3 ceramics", *Ceramica*, **66** [377] (2020) 65–73.
42. C.G. Sammis, M.F. Ashby, "The failure of brittle porous solids under compressive stress states", *Acta Metall.*, **34** [3] (1986) 511–526.
43. S. Meille, M. Lombardi, J. Chevalier, L. Montanaro, "Mechanical properties of porous ceramics in compression: On the transition between elastic, brittle, and cellular behavior", *J. Eur. Ceram. Soc.*, **32** [15] (2012) 3959–3967.
44. M.F. Ashby, C.G. Sammis, "The damage mechanics of brittle solids in compression", *Pure Appl. Geophys.*, **133** [3] (1990) 489–521.